geosciences

MDPI

Article

Distribution of Naturally Occurring Asbestos in the Mitrovica Region: Geochemical and Mineralogical Characterization

Bahri Sinani [1], Blazo Boev [1], Arianit A. Reka [2,3], Berat Sinani [1] and Ivan Boev [1,*]

1 Department of Environmental Engineering, Faculty of Natural and Technical Science, University "Goce Delchev", Shtip, 2000, North Macedonia; bahri.31326@student.ugd.edu.mk ; blazo.boev@ugd.edu.mk; berat.sinani@umib.net
2 Department of Chemistry, Faculty of Natural Sciences and Mathematics, University of Tetova, Tetovo 1200, North Macedonia; arianit.reka@unite.edu.mk,
3 Albanian Unit of Nanoscience and Nanotechnology, NanoAlb, Academy of Sciences of Albania, Fan Noli Square, Tirana 1000, Albania
* Correspondence: ivan.boev@ugd.edu.mk

Abstract

This study investigates the presence of naturally occurring asbestos (NOA) in the Bajgora region of Mitrovica, Republic of Kosovo. Rock samples were collected and analyzed using X-ray powder diffraction (XRPD) and scanning electron microscopy coupled with energy-dispersive X-ray spectroscopy (SEM/EDX). The analyses confirmed the presence of the chrysotile mineral, which is part of the asbestos mineral family, while the minerals of the serpentine group, lizardite and antigorite, were identified. Also, in the last sample, in the flyschite sandstone formations, quartz was identified. XRPD enabled the identification of mineral phases, while SEM/EDX provided detailed morphological and chemical characterization, essential for confirming asbestos structures. The detection of asbestos near residential areas raises serious public health concerns, as airborne fibers may be inhaled during routine daily activities. Exposure to these fibers is linked to severe diseases, including asbestosis and mesothelioma. These findings highlight the need for continued monitoring and comprehensive assessment of asbestos contamination in the Bajgora region. The findings point to the need for continuous monitoring and comprehensive assessment of the Bajgora region for asbestos contamination. Furthermore, the ecological risks to human health resulting from the dispersion of asbestos mineral fibers in the soil, where their presence may be found in surface waters and in the air, these fibers represent a significant environmental risk that requires urgent attention by establishing a monitoring system for the benefit of public health.

Keywords: asbestos; Bajgora region; XRPD; SEM/EDX; lizradite; antigorite; quartz; risk; environment

Academic Editor(s): Lev V. Eppelbaum

Received: 2025-08-04
Revised: 2025-08-19
Accepted: 2025-08-22
Published: date

Citation: Sinani, B.; Boev, B.; Reka, A.A.; Sinani, B.; Boev, I. Distribution of Naturally Occurring Asbestos in the Mitrovica Region: Geochemical and Mineralogical Characterization. *Geosciences* **2025**, *15*, x. https://doi.org/10.3390/xxxxx

1. Introduction

Asbestos is a collective term for six naturally occurring silicate minerals, primarily from the serpentine and amphibole groups, that share a fibrous crystalline structure [1]. These varieties include chrysotile, amosite, crocidolite, tremolite, anthophyllite, and actinolite [2].

Asbestos typically occurs in a fibrous or tubular form, which can be easily separated into thin fibers due to its crystalline structure [3]. Due to its durable nature and ability to

withstand high temperatures and chemicals, asbestos has been widely used in various industrial environments historically [4]. Despite its health risks, asbestos has historically been valued for its favorable properties, including heat resistance and durability [2].

Exploitation of asbestos as ACM (asbestos-containing materials) began between 1860 and 1875, and these materials were used until the 1970s, when they were recognized as posing significant health risks [5]. Historical records indicate that nearly every country has experienced a period of widespread asbestos use [6].

Although its health risks are well-documented, asbestos is still in use today [7]. Asbestos-containing products continue to be marketed and sold in many countries [8].

During the decades of widespread use, asbestos fibers were released into the air, contributing to environmental pollution and increasing the likelihood of exposure-related diseases. Among the most common health consequences of asbestos fiber exposure are lung cancer, respiratory tract irritation, and breast cancer [9].

The widespread use of asbestos has seriously affected human health. Prolonged inhalation of asbestos particles is associated with diseases such as asbestosis, lung cancer, and the frequently reported mesothelioma. In response, European nations have implemented strict regulations or complete bans on asbestos use. Italy, for instance, enacted a full ban relatively late under Law 257/1992 [10].

Asbestos has been classified as a carcinogenic substance (Group 1) by the International Agency for Research on Cancer [11]. Fibrous minerals are similarly classified by the IARC as substances-carcinogenic to humans (Group 1) [3].

Increasing scientific research continues to highlight the serious health risks associated with asbestos exposure, particularly when safety measures are inadequate in asbestos-related environments [12].

Asbestos-related diseases typically manifest after long latency periods. These diseases usually have long latency periods, ranging from 15 to 60 years, which complicates early diagnosis and underscores the need for preventive measures and long-term health monitoring [13].

Healthcare professionals and researchers have increasingly reported epidemiological indicators of asbestos-related diseases [13].

The presence of elements in asbestos-containing samples—especially heavy metals within engineered mineral particles (EMPs)—enhances their toxic potential. These elements can contribute to the development of lung cancer if released into the body after inhalation [3].

Most previous research has focused on occupational exposure to asbestos, assessing the risks of asbestos-containing products such as water supply pipes, and their subsequent environmental impacts on surrounding ecosystems and communities [14].

In the study area, mining operations that disturbed geological formations containing asbestos have led to the release of hazardous fibers into the environment, posing long-term public health concerns [14].

Air pollution from asbestos fibers remains a serious and ongoing threat to public health in the area [15].

The use of XRPD and SEM is essential for the research and detection of asbestos fibers [4]. Advanced methodologies enable precise identification and mapping of fibers, which are essential for accurate risk assessment and effective public health interventions. This study aims to contribute to this field by establishing a comprehensive database on the extent and sources of asbestos fiber contamination in the samples analyzed [16]. This database will support both scientific understanding and public health efforts in affected regions [16].

The study also seeks to raise awareness among the public and the broader community about the health risks associated with asbestos exposure, which can lead to serious asbestos-related diseases [3].

By confirming the presence of asbestos in this region, our research will contribute to further studies and help guide preventive strategies to protect the health and well-being of the local population [15].

Given the health risks associated with exposure to naturally occurring asbestos minerals, there is an urgent need for comprehensive, evidence-based assessments that prioritize the healthcare of residents in the Bajgora region. This research will serve as a catalyst for the systematic collection of reliable and professional data, aimed not only at advancing scientific understanding but also at safeguarding the health and well-being of the local population [14].

The International Agency for Research on Cancer (IARC), under the auspices of the World Health Organization (WHO), has classified all forms of asbestos as carcinogenic and posing a serious health risk to humans [2].

The main objective of this research is to address the environmental and complex issue of the presence and subsequent contamination with asbestos in the Mitrovica region, focusing on the Bajgora area and the villages around it.

Natural asbestos (NAA) is not only a geological concern, but it also poses a long-term ecological as well as toxicological risk. Rocks containing asbestos are exposed to us by many various factors such as natural erosion, mining activities, infrastructure development, while all these activities release microscopic fibers that are released into the soil, water, and atmosphere.

These fibers are non-degradable in the environment and have a lifespan of decades [11]. Unlike occupational exposure, which is limited in scope and time, exposure to NAA in natural environments is uncontrolled and has a negative impact on the population of the region, including residents, farmers, children, tourists, pets, etc.

The Bajgora region, due to its nature with serpentine formations and rocks and various geological formations, represents a particularly vulnerable landscape. Seasonal climate changes, heavy rains creating erosion, high snow levels, and wind can help disperse fibers, spreading contamination beyond the initial source site. Evidence from similar geological settings (e.g., El Dorado County, California; Broni, Italy; and the Cappadocia region of Turkey) has linked natural asbestos to high rates of mesothelioma and asbestosis in populations that are not occupationally exposed [17].

Furthermore, the presence of chrysotile fibers in the air can travel considerable distances, entering homes, food products, and even water reservoirs. This study provides the mineralogical basis necessary to begin ecological risk mapping and long-term monitoring plans in the Mitrovica region.

2. Methodology of Research

This research on the distribution of asbestos in the Bajgora region is structured in two main phases.

- Identification of the presence of asbestos in this area;
- Determination of asbestos type and its characteristics through advanced instrumental methods.

The Bajgora region, which lies in the northern part of Kosovo, is characterized by a wide spread of ultrabasic rocks, which appear mainly in the form of serpentinite, often heavily altered. This region, in addition to its geological importance, is also distinguished as an area with high potential for recreation and mountain tourism, due to its attractive natural landscape and favorable climatic conditions.

Fieldwork Methodology: The field component of this study commenced with the systematic collection of base rock samples, each accompanied by a comprehensive geological description to document site-specific characteristics [18]. The methodology employed for the identification of naturally occurring asbestos (NOA) in the study area was structured into several key phases: the recognition of asbestos-bearing lithologies; detailed observation and documentation of relevant geological features; construction of a high-resolution geological map; and precise determination of sampling locations using established geospatial criteria [19,20].

All sampling activities were conducted in accordance with internationally recognized standards and protocols to ensure the scientific integrity, reproducibility, and reliability of the collected data [21]. Particular attention was given to the selection of representative samples that reflect the prevailing geological conditions and are suitable for subsequent analytical procedures, including scanning electron microscopy (SEM, VEGA3) and X-ray powder diffraction (XRPD, Panalytical) analysis [22].

Visual identification: The sampling methodology was primarily focused on ultrabasic geological formations, with particular emphasis on serpentinized rocks-environments in which the presence of naturally occurring asbestos has been previously documented, as illustrated in Figure 1. Visual identification of asbestos fibers was undertaken with care, and particular attention was given to mineralized streaks and zones exhibiting clear evidence of asbestos within these formations, geological ruler presents vein of antigorite and in the right red line presents the vein of lizardites.

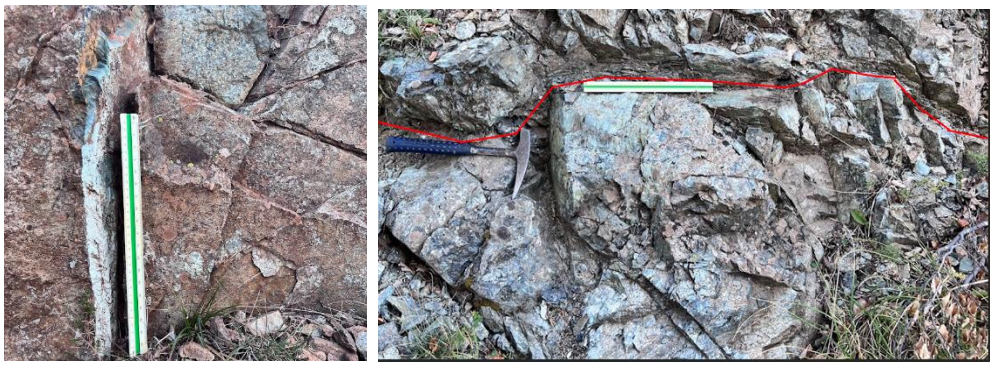

Figure 1. Evidence of asbestos fiber presence at the surface, indicating potential environmental exposure risks.

Laboratory Method:

To conduct this study, two advanced analytical techniques were employed:

- Scanning Electron Microscope equipped with Energy-Dispersive X

Scanning Electron Microscope was used to examine the microstructural features of the collected samples. Elemental composition was determined using the integrated EDX (energy dispersive X-ray analysis) detector.

SEM/EDX analyses were performed at the Center for Scientific and Technological Research and Applications (ARTMER) of Bülent Ecevit University in Zonguldak, using an FEI Quanta FEG 450 model. Measurements were performed in BSE (back scattered electron) mode under LFD LOV vacuum conditions, with an accelerating voltage ranging between 15 and 20 kV. A conductive gold (Au) layer was used to prepare the samples for SEM/EDX analysis, while carbon (C) was used to bond the samples to polymers for mounting.

Representative samples were selected for detailed SEM analysis, which included morphological characterization, elemental profiling, and spectral detection of primary components [23]. Prior to analysis, the samples were ground and sieved through a 63 μm

mesh to ensure homogeneity and optimize spectrometric resolution. For each sample, 50 g of material were processed, from which 2 g were homogenized and submitted for laboratory analysis.

- X-ray Powder Diffraction (XRPD)

This research was carried out at the BEU ARTIMER X-Ray Laboratory utilizing a Panalytical Empyrean model instrument. The measurements were performed under conditions of 45 k, 45 mA power, employing a reflection–transmission spinner stage, with a scan range of 10–90° and an incremental step size of 0.0013°. The collected data were processed using the High Score 3 Plus software, and the findings are presented and discussed in the following section

The results revealed variable asbestos content in samples 1, 2, and 3, while no asbestos phases were identified in sample 4. The global refinement parameters Re and Rp were below the commonly accepted threshold (R < 10) and were closely aligned, indicating strong consistency and high reliability between the SEM and XRPD (Rietveld) methods.

This combined analytical approach has demonstrated a high degree of accuracy in identifying fine mineral structures and crystalline phases, and is widely recognized and recommended for environmental studies, including by the U.S. Environmental Protection Agency (EPA, 1993) [24].

The purpose of this analysis was to identify specific asbestos mineral subtypes and any co-occurring elements typically associated with asbestos minerals [19], such as magnesium (Mg), silicon (Si), and oxygen (O).

3. Study Area

In this study, samples were collected from base rocks, particularly serpentinites, where the occurrence and distribution of asbestos fibers were observed in several cases.

The presence of asbestos fibers in natural geological environments is recognized as a serious global public health concern [25]. Asbestos is a naturally occurring mineral that forms as fibrous structures, which can be separated into thin threads [26].

Serpentinite rocks have a geologically complex origin, formed through the process of serpentinization of ultramafic rocks, primarily composed of pyroxenes and olivine, originating from the Earth's mantle. The main mineralogical phases within serpentinites include chrysotile, lizardite, and antigorite [5].

This research confirms the presence of asbestos within the bedrock by examining the mineralogical context and geological relationships, consistent with findings from previous studies [14]. Through field observations and laboratory analyses, the geology of the Bajgora region was mapped and the occurrence of asbestos fibers in the environment was substantiated [14].

Geographically, the Bajgora region is located in northeastern Kosovo. It lies east of Mitrovica, west of Podujeva, and northeast of Vushtrri, forming part of the southern extension of the Kopaonik Mountains. The asbestos-related investigation covered several villages, including Bajgora, Kaçandoll, Rrëzhana, Bare, Selac, and Kovaçicë [27].

Tectonically, the region belongs to the Vardar Zone, which is traditionally subdivided into the Western, Central, and Eastern Vardar Zones [28]. Based on early geological research, the study area is positioned within the Central Vardar Zone [27, 29]. This tectonic setting is critical for understanding the genesis and spatial distribution of asbestos-bearing formations [29].

The Central Vardar Zone in the study area is primarily composed of serpentinite rocks. To the east, limestone and marlstone dominate, while the western and southwestern parts are mostly composed of green schists. Additionally, the western zone of the

study area features volcanogenic-sedimentary formations, as illustrated in the geological map presented in Figure 2.

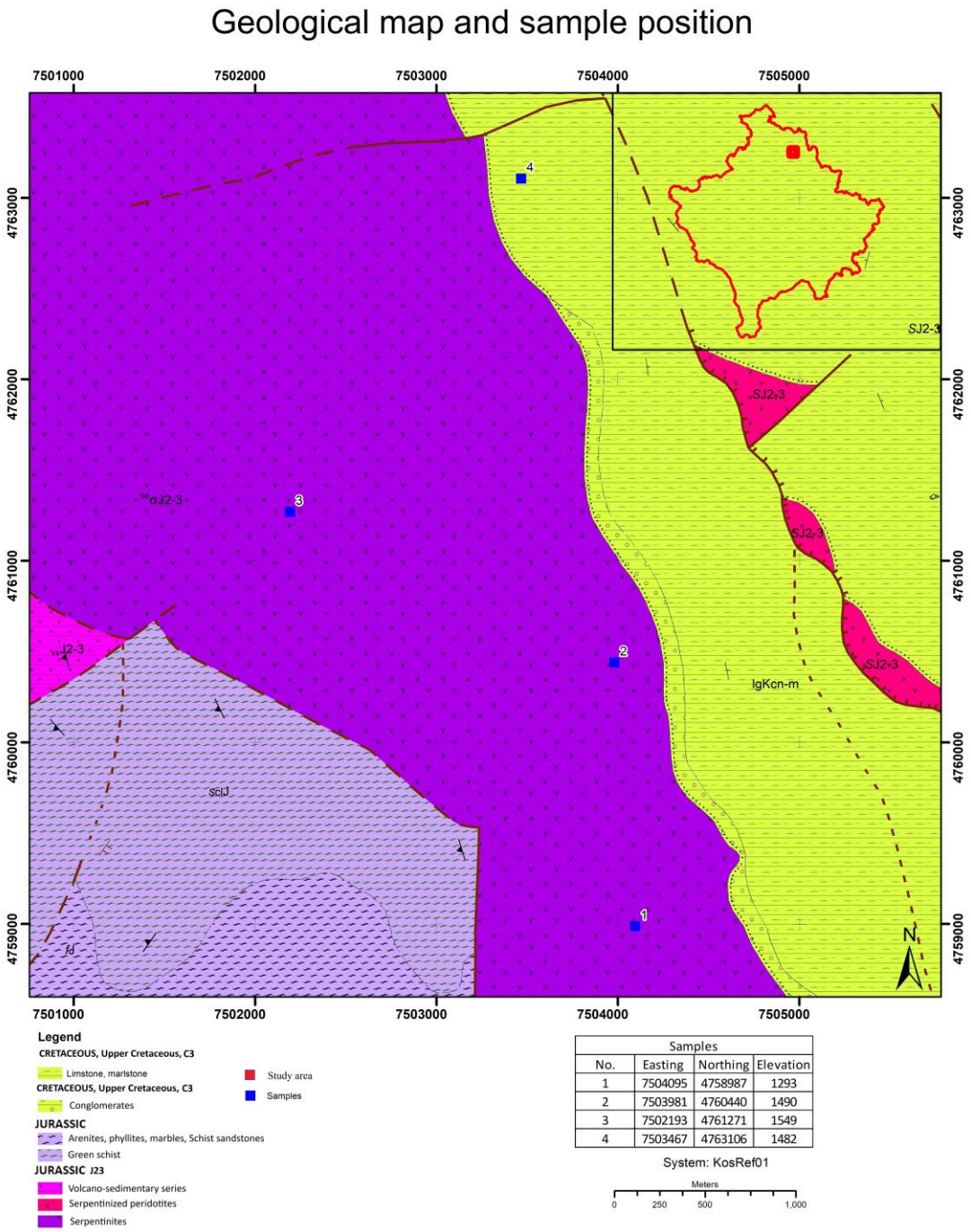

Figure 2. Geological map of the study area [30].

Figure 2 presents the geological map of the study area [30], which is situated in the northern part of Kosovo.

Geological mapping: was carried out through the interpretation of existing geological maps [31], enabling the identification of zones with high potential for asbestos occurrence. These areas were delineated based on lithological boundaries—specifically between ultrabasic and calcareous-sandstone formations to the east, and greenschist units to the west of the Bajgora region.

Field observations and sampling confirmed that the geological structure of the study area is composed primarily of serpentinite rock formations, along with sandy flysch, marble conglomerates, phyllites, greenschists, and a westward-extending sequence of volcanogenic-sedimentary units [32]. In many areas, serpentinization is expressed through parallel fault systems that intersect and form a network of structural dislocations [7].

In the eastern section of the study area, flysch formations are in tectonic-erosive contact with limestone; the contact is especially visible at the northeastern border of the Kaçandolli Massif, where the serpentine series are also in contact with sandy flysch and sandy conglomerates. In the southwestern sector, green shales interbedded with phyllites and marble dominate the stratigraphy. Meanwhile, the western portion of the study area features a transition zone where serpentinites, green shales, and volcanogenic-sedimentary formations converge—continuing in the direction of the village of Selac [33].

The serpentinite formations of the Jurassic period J2-3 come into tectonic contact with the conglomerate, limestone, and marlstone formations of the Cretaceous geological period K2 [7].

Hydrogeological parameters must also be taken into consideration, particularly in areas where asbestos is exposed at or near the surface. In such regions, the movement of surface and groundwater can facilitate the mobilization and transport of asbestos fibers into the broader environment, potentially increasing human exposure risks [34].

4. Results and Discussions

The data presented in Table 1 summarize the results of SEM-EDAX analysis for samples 1, 2, 3 and 4, where the table includes the elemental composition of each sample, expressed in both weight percent (Wt%$_i$) and atomic percent (At%$_i$), while Table 2 presents the composition of oxides by % in the analyzed samples from the elemental weight percent (Wt%$_i$) obtained by SEM-EDS.

These values were calculated using standard formulas specific to each parameter, providing a reliable representation of the chemical composition of the analyzed samples.

$$At\%_i = \left(\frac{n_i}{\sum n_j}\right)\cdot 100 \quad Wt\%_i = \left(\frac{m_i}{\sum m_j}\right)\cdot 100$$

n_i = number of atoms of a specific element
m_i = mass of element i
$\sum n_j$ = total number of atoms of all elements
$\sum m_j$ = total mass of all detected elements

Table 1. Elemental composition of the analyzed samples as determined by scanning electron microscopy (SEM-EDX).

Sample 1.			**Sample 2.**		
Element	Wt%	At%	Element	Wt%	At%
O	65.82	75.52	O	63.85	73.93
Mg	20.49	15.49	Mg	21.48	16.37
Al	1.60	1.09	Al	1.47	1.00
Si	12.09	7.90	Si	13.20	8.70
Sample 3.			**Sample 4.**		
Element	Wt%	At%	Element	Wt%	At%
O	63.71	73.87	O	65.76	77.51
Mg	20.79	15.87	Mg	1.09	0.82
Al	1.80	1.24	Al	9.76	6.63
Si	13.55	8.95	Si	22.85	14.85

Ca	0.16	0.07	K	0.54	0.19

Table 2. Composition of oxides (% by weight) in the analyzed samples recalculated from the elemental weight percentages obtained by SEM-EDS.

Oxides %	Sample 1	Sample 2	Sample 3	Sample 4
MgO	54.05	53.45	51.39	2.59
Al_2O_3	4.81	4.17	5.07	26.43
SiO_2	41.14	42.38	43.21	70.05
CaO	0	0	0.33	0
K_2O	0	0	0	0.93

Table 2 presents the main oxide composition (Wt%$_i$) for the four analyzed samples. Samples 1 to 3 show a stable composition, dominated by MgO (51.39–54.05%) and SiO_2 (41.14–43.21%), with only small amounts of Al_2O_3 (4.17–5.07%) and traces of CaO (0.33% only in sample 3). This MgO–SiO_2 dominance clearly reflects the typical geochemistry of serpentinite minerals. Sample 4 differs significantly from the first three, being characterized by very high SiO_2 (70.05%) and significant Al_2O_3 (26.43%), while MgO is very low (2.59%). The presence of K_2O (0.93%) in this sample indicates a potassium (K)-containing mineral composition in the muscovite presented in this sample ($KAl_2(AlSi_3O_{10})(OH)_2$).

Sample 1. The mineralogical characteristics of sample 1 are presented below and illustrated in Figure 3. A detailed analysis of its composition and structure was conducted to identify the presence of asbestos-related phases and associated mineral components.

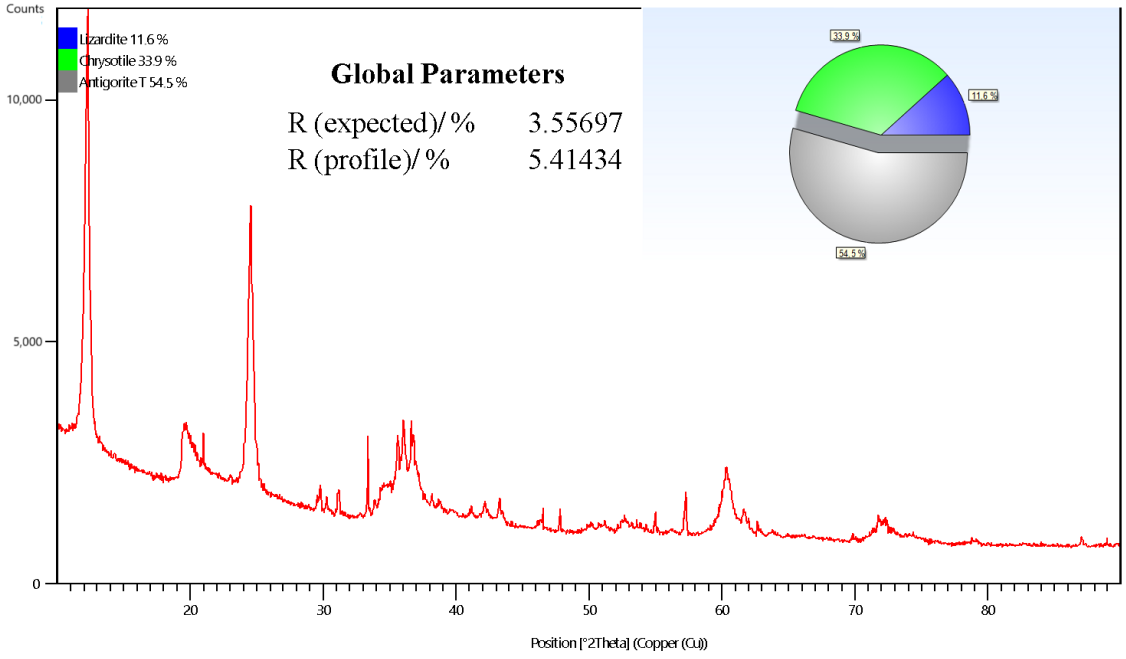

Figure 3. X-ray diffraction (XRD) pattern of sample 1.

The mineralogical characteristics of sample 1 are presented below and illustrated in Figure 3. X-ray diffraction (XRD), interpreted using the Rietveld method, provided a detailed characterization of the sample's mineralogical composition. The analysis identified three main minerals of the serpentine group: antigorite (54.4%), chrysotile (33.9%), and lizardite (11.6%). The diffraction pattern clearly shows the characteristic reflections of each phase: chrysotile exhibits sharp peaks at 12.0°, 24.2°, and 36.5° 2θ; antigorite is characterized by broader peaks at 11.4°, 19.3°, and 32.4° 2θ, typical of its disordered layer structure;

while lizardite is identified by reflections at 19.7° and 55.2° 2θ, indicating its fine-grained nature. The quantitative analysis confirms antigorite as the dominant phase, followed by chrysotile and then lizardite.

The concentrations of atoms in the regular formulas and the formulas that appear in the minerals identified in sample 1, based on the powder diffraction file, are summarized in Table 3.

Table 3. Table shows us the regular chemical formulas and the formulas generated by spectrometry for sample 1.

Ref. Code	Mineral Name	Chemical Formula	Concentration [%]
98-002-3813	Lizardite	$H_4Mg_3O_9Si_2$	11.6
98-041-3633	Chrysotile	$H_4Mg_3O_9Si_2$	33.9
98-009-5342	Antigorite T	$H_{50}Mg_{39}O_{120}Si_{28}$	54.4

Table 3 shows the regular chemical formulas and the spectrometrically generated formulas of the minerals for sample 1; the first row presents the ideal chemical formula, while the second row presents the chemical formulas as given by the ICDD database and reflects the measured stoichiometry of the sample and the idealized formula of the lizardite, chrysotile and antigorite-T minerals.

Figure 4 presents the morphological characteristics of the sample as observed through scanning electron microscopy (SEM).

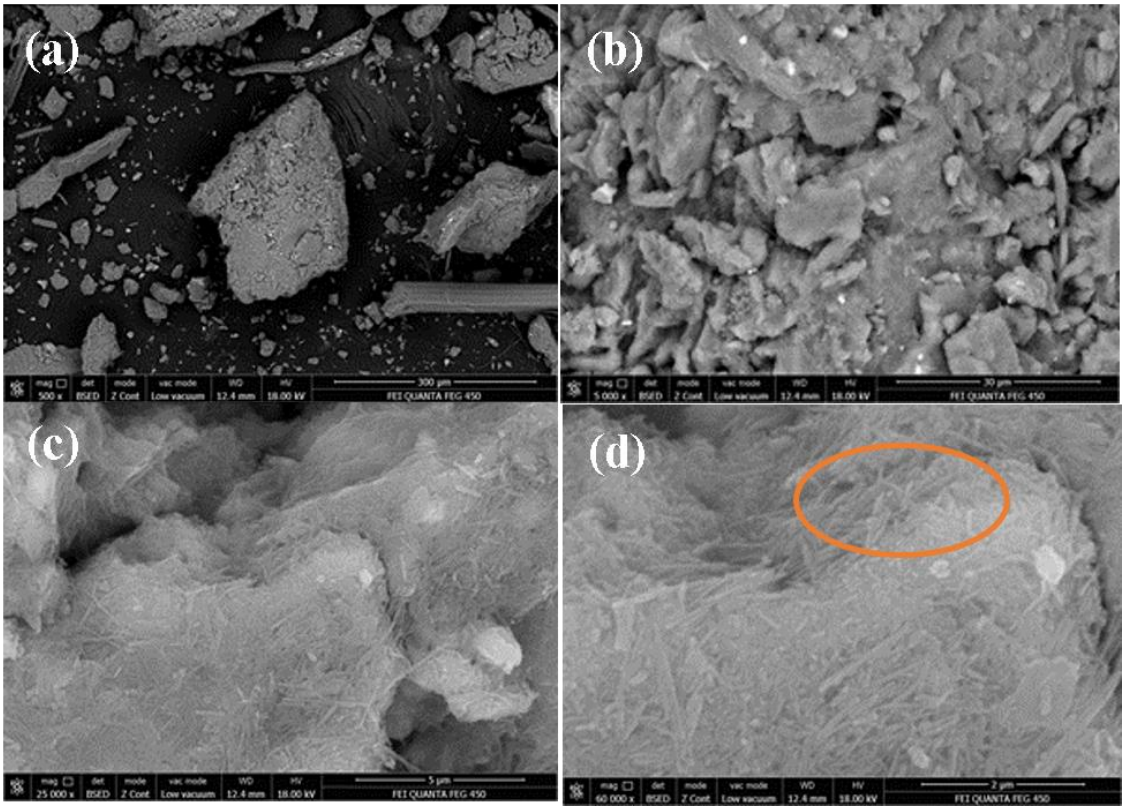

Figure 4. SEM image of sample 1: a) 300 μm, b) 30 μm, c) 5 μm, d) 2 μm

SEM micrographs of sample 1, Figure 4, show distinct morphological characteristics at different magnifications. At low magnification 4a, the surface shows angular and irregular particles of various sizes, revealing the structural composition of the sample. At intermediate magnification 4b, the plate-like and broken particles become more visible

along the surface change where lizardite is observed in the form of plates. Higher magnification images, as shown in 4c , show elongated, thin and fibrous structures but of the laminar type and we are dealing with Antigorite. At very high magnification 4d, these fibers are clearly distinguished with a pronounced needle-like shape and high aspect ratio, emphasized in the encircled region, confirming the presence of fibrous textures typical of minerals associated with chrysotile.

Sample 2. The mineralogical composition of sample 2 is presented below and illustrated in Figure 5, based on the results of detailed phase identification and structural analysis.

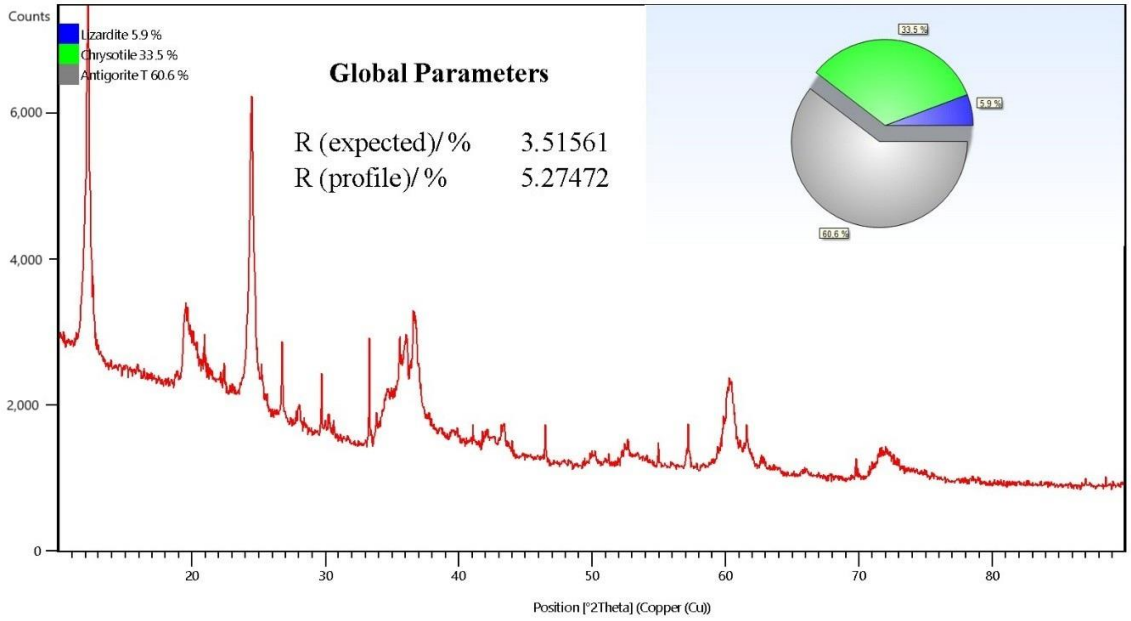

Figure 5. X-ray diffraction (XRD) pattern of sample 2.

The mineralogical composition of sample 2 is illustrated in Figure 5. The X-ray diffraction (XRD) pattern, refined by Rietveld analysis, reveals the presence of three serpentine-group minerals: antigorite (60.6%), chrysotile (33.5%), and lizardite (5.9%). The diffraction exhibits distinct reflections attributed to these phases. Chrysotile is marked by prominent peaks at 12.0°, 24.2°, and 36.5° 2θ, while antigorite shows broader and more diffuse reflections at 11.4°, 19.3°, and 32.4° 2θ, typical of its irregularly layered structure. Lizardite is identified by much weaker peaks at 19.7° and 55.2° 2θ, reflecting its softer and less crystalline nature. Quantitative phase analysis confirms antigorite as the dominant component in sample 2, followed by chrysotile, with only a minor contribution from lizardite.

The concentrations of atoms in the regular formulas and the formulas that appear in the minerals identified in sample 2, based on the powder diffraction file, are summarized in Table 4.

Table 4. Table shows us the regular chemical formulas and the formulas generated by spectrometry for sample 2.

Ref. Code	Mineral Name	Chemical Formula	Concentration [%]
98-002-3813	Lizardite	$H_4Mg_3O_9Si_2$	5.9
98-041-3633	Chrysotile	$H_4Mg_3O_9Si_2$	33.5
98-009-5342	Antigorite T	$H_{50}Mg_{39}O_{120}Si_{28}$	60.6

Table 4 presents three serpentine minerals in sample 2, namely lizardite, chrysotile and antigorite T, where the first row of the mineral contains the regular formulas of each mineral, while the second row presents the formulas identified through XRD analysis and the link to their codes in the ICDD (powder diffraction file) database:

Figure 6 presents the morphological characteristics of sample 2 as observed through scanning electron microscopy (SEM).

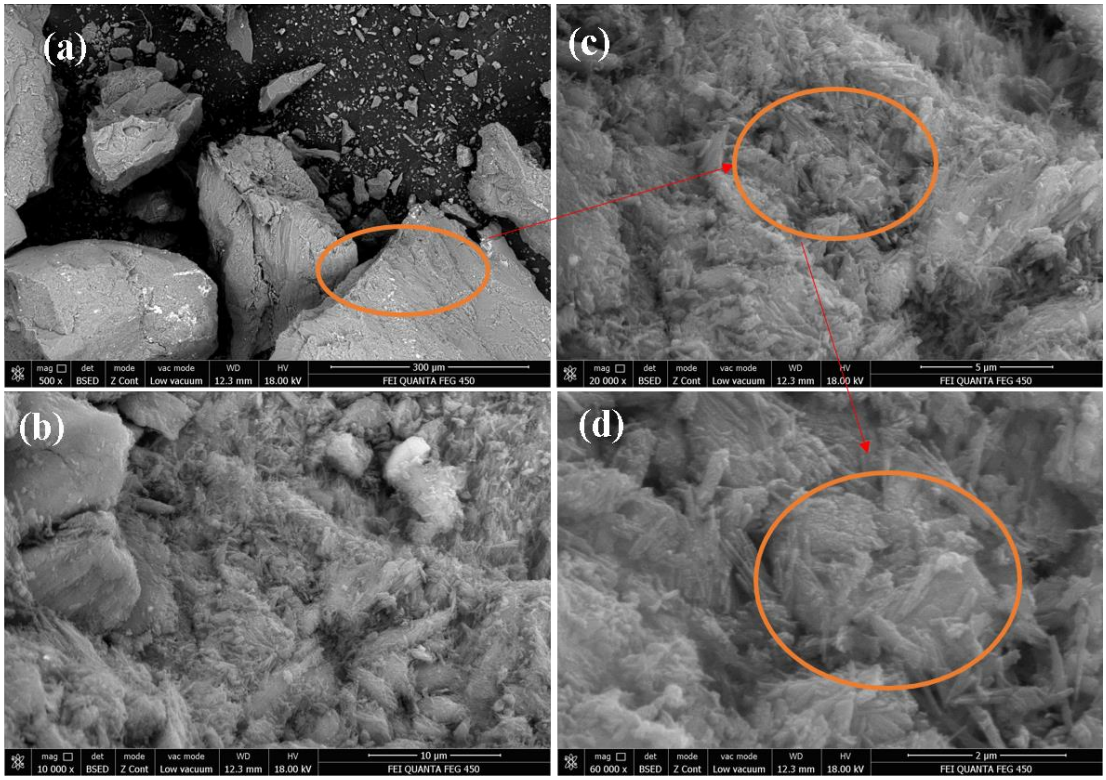

Figure 6. SEM images of sample 2: a) 300 μm, b) 10 μm, c) 5 μm, d) 2 μm

SEM images of sample 2 shown in Figure 6 reveal distinct morphological features at multiple magnifications. At low magnification 6a, the surface consists of large angular rock fragments with localized areas of fibrous material visible along the edges. At intermediate magnification 6b, a mixture of flat textures and early fibrous formations is observed. At high magnification 6c, laminar bundles with dense fibrous strumas are clearly visible, arguing for the presence of antigorite, which are intertwined and elongated. At the highest magnification 6d, individual fibers are clearly distinguished with a pronounced needle-like shape, confirming the presence of the fine fibrous morphologies typical of chrysotile-type minerals, while lizardite appears in SEM as very fine microplates attached to the surface, creating a dense matrix.

Sample 3. The mineralogical characteristics of sample 3 are presented below and illustrated in Figure 7, based on detailed phase identification and structural analysis.

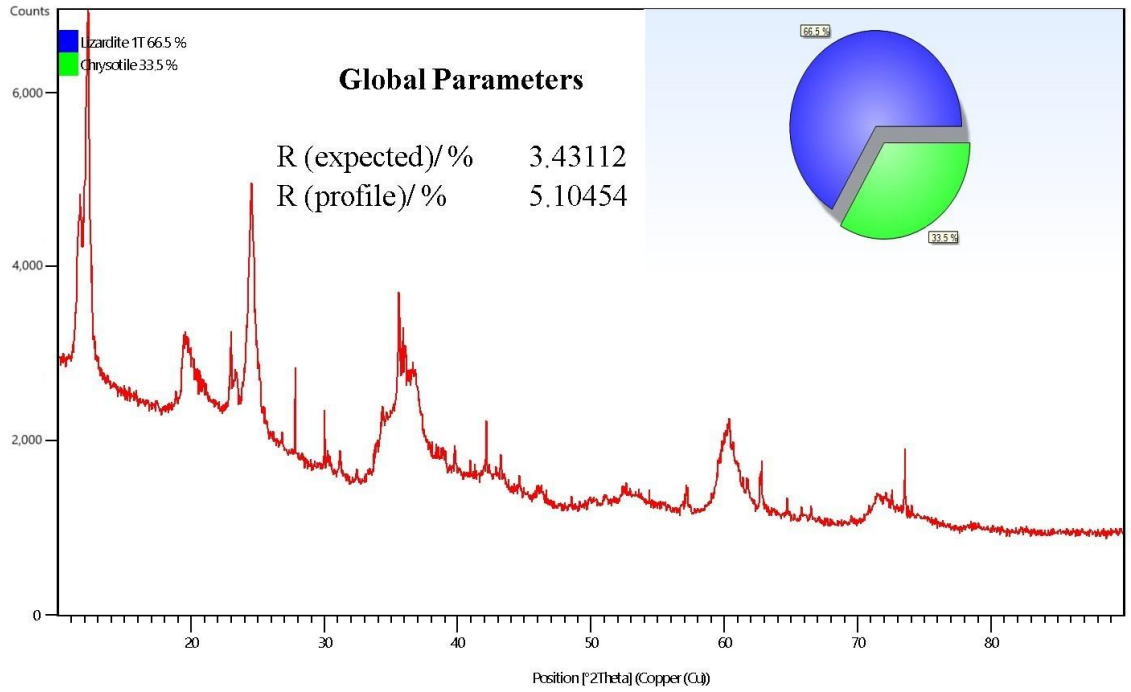

Figure 7. X-ray diffraction (XRD) pattern of sample 3.

The mineralogical composition of sample 3 is illustrated in Figure 7. The X-ray diffraction (XRD) pattern, refined using Rietveld analysis, reveals the presence of two serpentine group minerals: lizardite-1T (66.5%) and chrysotile (33.5%). The diffraction exhibits distinct reflections corresponding to these phases. Lizardite-1T is characterized by strong peaks at 12.0°, 24.2° and 36.5° 2θ, indicating its well-ordered structure. Chrysotile, on the other hand, is marked by sharp reflections at similar positions, but with slight shifts in peak intensity, reflecting changes in its fibrous crystalline morphology. Quantitative phase analysis confirms lizardite-1T as the dominant phase in sample 3, with chrysotile mineral making up the remainder.

The concentrations of atoms in the regular formulas and the formulas that appear in the minerals identified in sample 3, based on the powder diffraction file, are summarized in Table 5.

Table 5. Table shows us the regular chemical formulas and the formulas generated by spectrometry for sample 3.

Ref. Code	Mineral Name	Chemical Formula	Concentration [%]
98-008-7437	Lizardite 1T	$H_4Mg_3O_9Si_2$	66.5
98-041-3633	Chrysotile	$H_4Mg_3O_9Si_2$	33.5

Table 5 presents two minerals in serpentinite rocks such as lizardite and chrysotile where both minerals are polymorphs and have the same ideal chemical formula; the same formula is also presented to us after XRD analysis using the ICDD (powder diffraction file) codes specific to each element.

Figure 8 presents the morphological characteristics of sample 3 as observed through scanning electron microscopy (SEM).

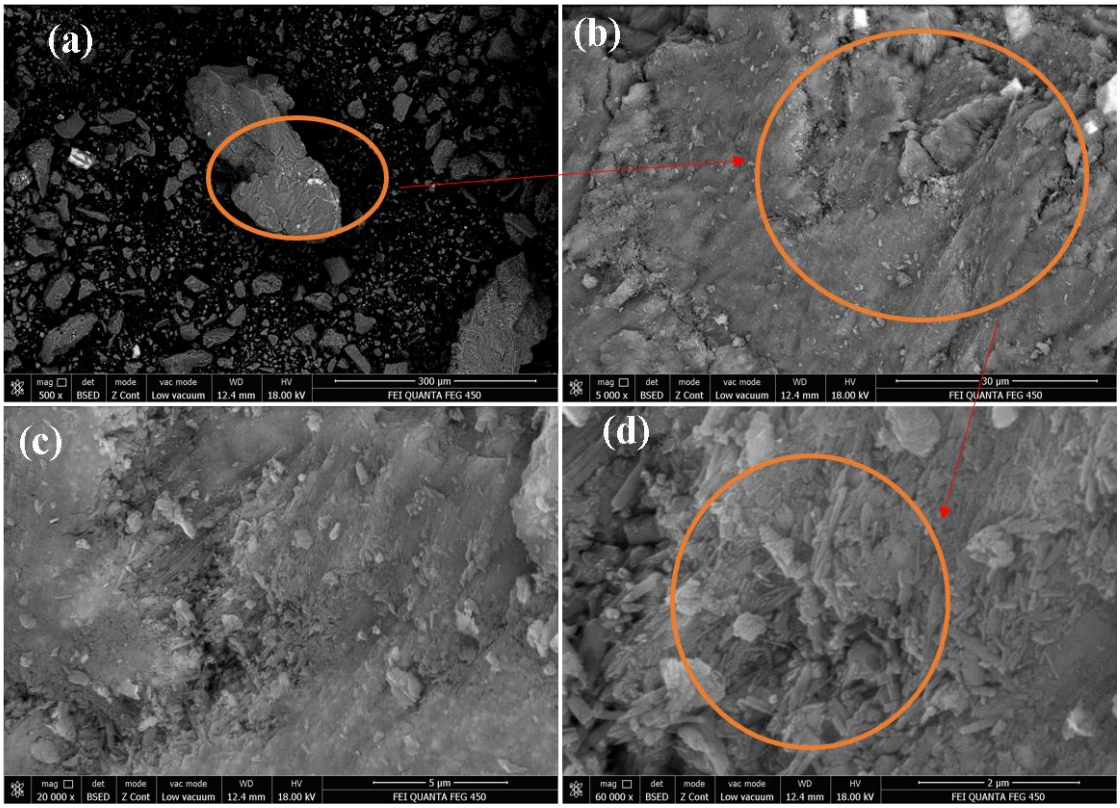

Figure 8. SEM image of sample 3: a) 300 μm, b) 30 μm, c) 5 μm, d) 2 μm

SEM images of sample 3 are shown in Figure 8. In the top-left image (Figure 8a), the general surface of the sample is seen with rock fragments of various sizes, with mostly angular and broken edges. In the top-right image (Figure 8b) at this level, plate and crushed structures are observed that make up the main matrix of the sample. The thin plates are joined and create uneven surfaces, forming a dense and fragmented texture typical of lizardite-1T, which appears as microplate aggregates. In the bottom-left image (Figure 8c), thin and long fibers are clearly distinguished. They appear scattered over the matrix of lizardite-1T, where some are visible as individual threads, while others are collected in small bundles. In the bottom-right image (Figure 8d) we clearly see thin, long and needle-like fibers with a high length-width ratio, which confirm the presence of chrysotile.

Sample 4. The mineralogical composition of sample 4 is presented below and illustrated in Figure 9, based on detailed phase identification and structural analysis.

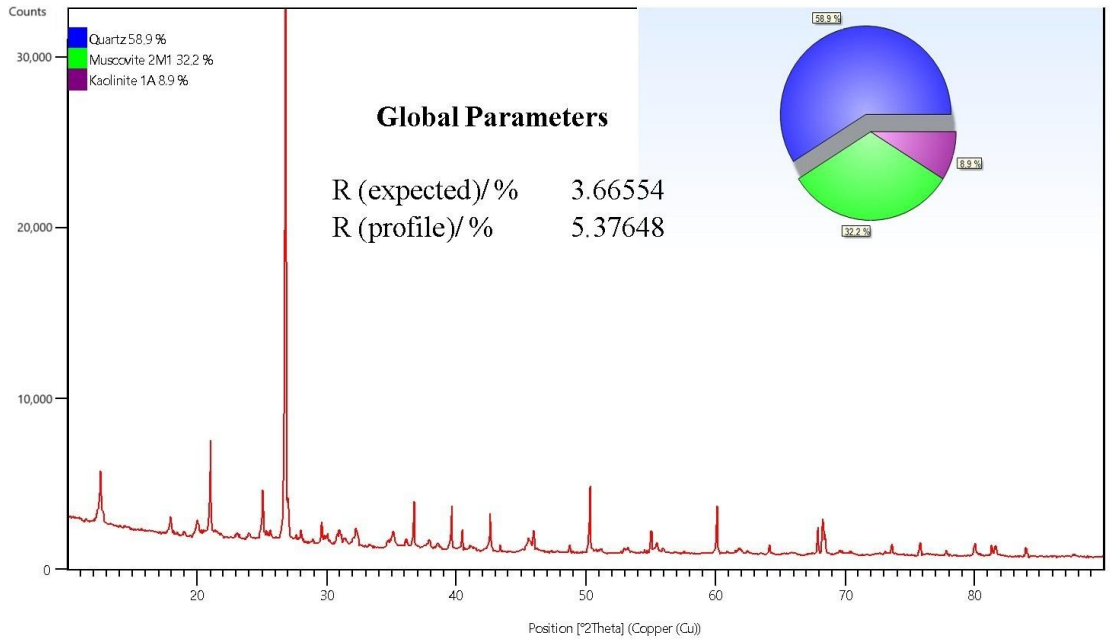

Figure 9. X-ray diffraction (XRD) pattern of sample 4.

The mineralogical composition of sample 4 is illustrated in Figure 9. The XRD diffraction pattern using the Rietveld method shows a mineral assemblage dominated by 58.9% quartz, 32.2% muscovite-2M1 and 8.9% kaolin-1A. The diffraction pattern shows sharp and intense peaks, especially in the strong quartz reflections at 26.6° 2θ, indicating a high degree of crystallinity. Muscovite is identified by its characteristic reflections in the 10–80° 2θ scan, and a higher order reflection at 45° 2θ, while the main peak at 8.9° 2θ is not recorded because it falls outside the measured range, while kaolinite is recognized by its diagnostic peaks at 12.3° and 24.8° 2θ, indicating the presence of a secondary alteration phase.

In quantitative terms, quartz appears as the dominant mineral, supported by significant amounts of muscovite and minor kaolinite, presenting a mineralogical composition typical of sedimentary metamorphic material.

The concentrations of atoms in the regular formulas and the formulas that appear in the minerals identified in sample 4, based on the powder diffraction file, are summarized in Table 6.

Table 6. Table shows us the regular chemical formulas and the formulas generated by spectrometry for sample 4.

Ref. Code	Mineral Name	Chemical Formula	Concentration [%]
98-015-6196	Quartz	O_2Si_1	58.9
98-020-2261	Muscovite 2M1	$H_2Al_{2.9}K_1O_{12}Si_{3.1}$	32.2
98-003-1135	Kaolinite 1A	$H_4Al_2O_9Si_2$	8.9

Table 6 presents three minerals with a pure silicate structure, where quartz is in between the regular formula and the XRD-analyzed formula but presented with different atomic arrangements. Muscovite is a mica or sheet mineral, variant 2M1 where it refers to the polymorph type related to the symmetry of the unit cell. The regular formula of muscovite differs from the formula as presented to us from the XRD readings using the ICDD

codes. Kaolinite is a common clay mineral. The ICDD formula is longer and presented differently, but is essentially the same as the regular formula.

Figure 10 presents the morphological characteristics of sample 4 as observed through scanning electron microscopy (SEM).

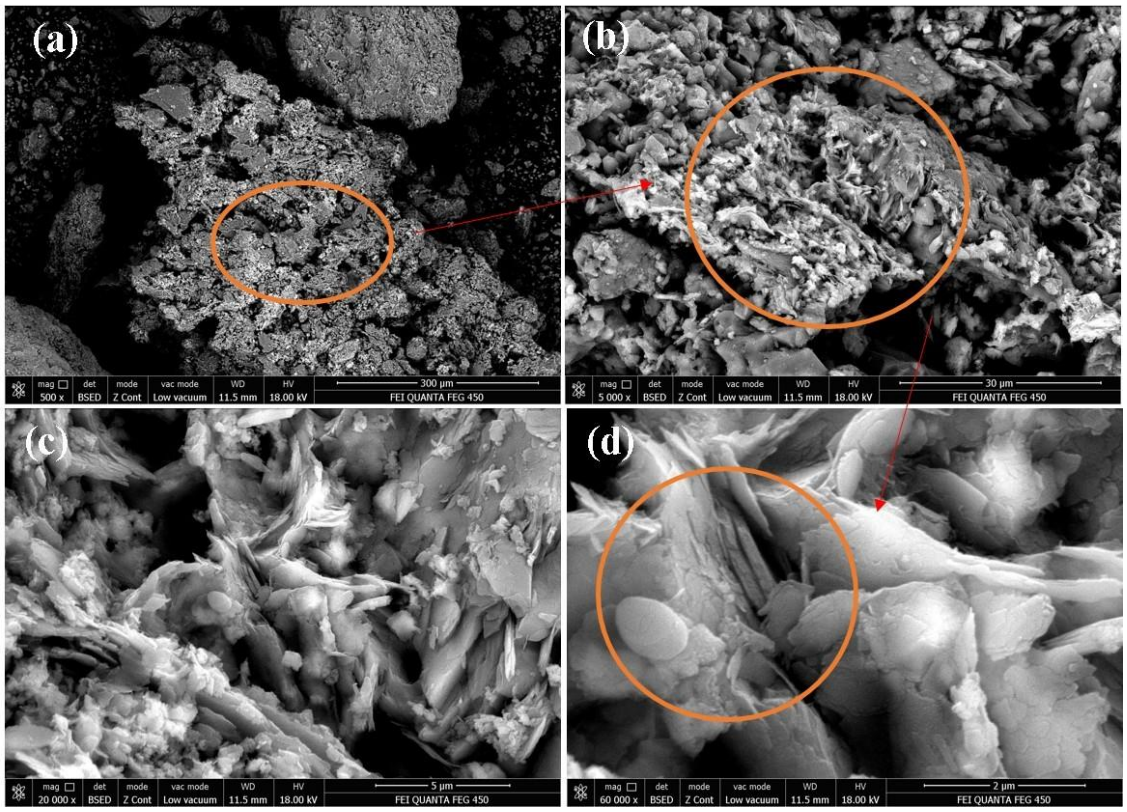

Figure 10. SEM image of sample 4: a) 300 µm, b) 30 µm, c) 5 µm, d) 2 µm

The SEM analysis of sample 4, as shown in Figure 10, from the top-left image (Figure 10a), SEM reveals large angular fragments with irregular edges and a heterogeneous grain distribution. The highlighted area shows clumps of sheet-like material, likely corresponding to muscovite plates intercalated within a matrix of fine particles.

The intermediate image (Figure 10b) shows well-defined sheet-like structures that are layered and partially broken, confirming muscovite as presented with red circle, which as a sheet silicate is formed by broad lamellae visible in SEM, where in the cracks of this material silicate from kaolin appears as fine-grained material filling the spaces between the plates, while at higher magnification (Figure 10c), the layered textures at this level of silicate are more prominent. The muscovite plates are more clearly visible, overlapping and forming an intercalated fabric. The very high magnification images (Figure 10d) show clear sheet-like structures confirming the presence of muscovite with its characteristic layered morphology. The smooth coatings between and on the muscovite sheets are consistent with kaolinite, while the sharp-edged fractures visible in the background reflect the dominant quartz structure.

In Table 7, which presents the results of X-ray diffraction (XRD) analysis for four mineral samples, the mineral phases, their chemical formulas and percentages for each sample have been identified.

Table 7. The results on the percentage and mineralogical phase of minerals found in four samples.

Ref. Code	Mineral Name	Chemical Formula	Concentration [%]			
			Sample 1	Sample 2	Sample 3	Sample 4
98-002-3813	Lizardite	$H_4Mg_3O_9Si_2$	12	6	67	0
98-041-3633	Chrysotile	$H_4Mg_3O_9Si_2$	34	34	34	0
98-009-5342	Antigorite T	$H_{50}Mg_{39}O_{120}Si_{28}$	54	61	0	0
98-015-6196	Quartz	O_2Si_1	0	0	0	59
98-020-2261	Muscovite 2M1	$H_2Al_{2.9}K_1O_{12}Si_{3.1}$	0	0	0	32
98-003-1135	Kaolinite 1A	$H_4Al_2O_9Si_2$	0	0	0	9

The data in Table 7 show the composition of samples 1, 2 and 3 which are dominated by minerals of the serpentine group of rocks: lizardite, chrysotile and antigorite T. These minerals are closely related to the processes of hydrothermal alteration in ultramafic rock and often constitute the main phases of natural asbestos in a specific way, as chrysotile. Sample 4 has a different composition for the content where the dominant minerals are quartz and muscovite, as well as a small percentage of kaolinite 1A. This mineralogical profile gives us the clarity of a more siliceous origin in sample 4, unlike the ultramafic-serpentine nature of the first three samples.

Figure 11, presented below, shows us in detail the X-ray spectra (XRD) showing the mineralogical changes of the analyzed samples.

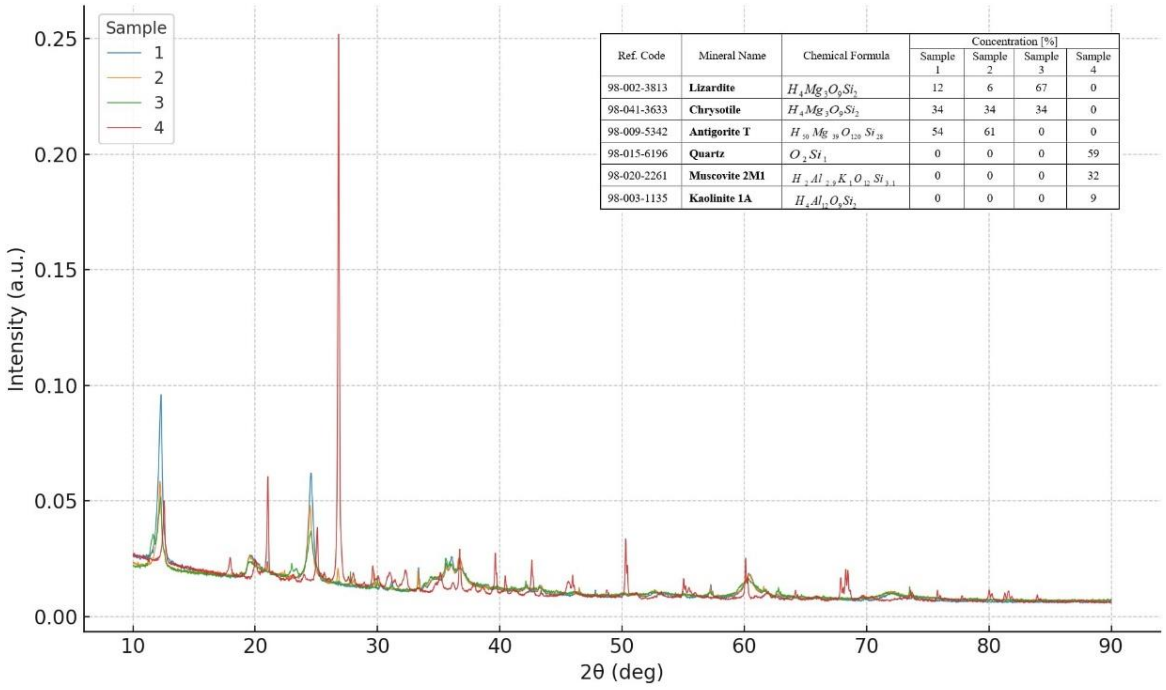

Figure 11. Shows the XRD spectra for the 4 analyzed samples.

Figure 11 shows the main mineralogical differences between the samples, where samples 1, 2 and 3 contain typical serpentine group minerals such as antigorite, chrysotile, lizardite, while sample 4 contains non-serpentine silicate minerals such as quartz, muscovite and kaolin.

X-ray diffractometric (XRD) analysis of the four samples shown in this graph reveals considerable similarity in peak positions and shapes, but with considerable differences in intensity, reflecting the mineralogical differences between the samples. All diffractograms exhibit main diffraction peaks in the range 10–30° 2θ to 60° 2θ, which are characteristic of serpentine group minerals and other associated components, depending on the geological setting.

The analysis shows that the high presence of chrysotile in most samples raises important issues for monitoring, due to the possible health and environmental implications related to exposure to asbestos fibers. On the other hand, sample 4 shows a different potential for use, as it is dominated by quartz and muscovite.

The presence of chrysotile, lizardite and antigorite in the analyzed samples indicates a high potential for the emission of fibrous particles from these minerals. These fibers, especially chrysotile, are known for their aerodynamic properties and stability and the ability to remain suspended in the air for long periods of time. In the Bajgora region, seasonal agricultural activities, recreational tourism and unregulated construction are increasingly increasing, which also increases the possibility of disturbing asbestos-rich soils, unintentionally releasing fibers into the environment that can be inhaled by local residents. Given the topographical features of the area, which has steep slopes and large relief differences, heavy rainfall and limited vegetation in some sections, allow the transport of fibers through runoff channels and surface waters. The risk of impact from surface waters on groundwater is easily possible, leading to contamination of drinking water or deposits on arable land, thus entering the food chain.

The ecological hazard of asbestos is presented by its resistance to chemical degradation, making natural attenuation impossible. Wildlife and livestock are also species at risk from exposure, especially in areas where the fibers are deposited in pastures. Previous studies in other regions affected by asbestos have shown that environmental exposure to NOA is associated with increased incidence of mesothelioma in women and children, populations that are not usually involved in industrial activities as presented in table 8. Therefore, it is essential that the Bajgora region be treated not only as a site of geological interest, but as an area of high ecological risk emergency that requires environmental risk management strategies. This includes the need to create buffer zones, regulate land use, conduct airborne fiber measurements and epidemiological studies of nearby populations.

Table 8. Summary of ecological and public health risks associated with naturally occurring asbestos (NOA) in the Bajgora region [35–39].

Exposure Pathway	Risk Description	Affected Compartments	Impacted Populations
Airborne dispersion	Asbestos fibers released through wind erosion, road construction, or agriculture	Ambient air	Residents, farmers, tourists, children
Surface water transport	Fibers washed into streams during rainfall and runoff	Rivers, irrigation canals	Communities downstream, agricultural zones
Soil retention	Accumulation in topsoil layers, especially in pastureland and cropland	Agricultural soil, grazing land	Farmers, livestock, food chain
Wind resuspension	Previously deposited fibers lifted back into	Atmospheric boundary layer	Entire local population

	the air during dry and windy conditions		
Groundwater migration	Potential for slow leaching of fibers into aquifers via fracture networks	Shallow aquifers	Rural households using groundwater
Uncontrolled land use	Infrastructure or development activities disturbing asbestos-rich rocks	Construction sites, slopes	Workers, construction crews, nearby inhabitants
Biodiversity impact	Chronic exposure to fibers may affect soil fauna or aquatic life	Terrestrial and aquatic habitats	Ecosystem health and ecological services

5. Conclusions

This study investigated four rock samples collected from the Bajgora region, three of which are derived from serpentinite formations and one from sedimentary rocks. The analytical results—especially from the first three samples—confirmed the presence of minerals with known toxicological potential, most notably chrysotile, a form of asbestos associated with significant health and environmental risks.

Quantitative analysis using XRD and SEM-EDX revealed the presence of serpentine minerals such as lizardite, lizardite-1T and antigorite-T, and the mineral chrysotile which belongs to the fibrous asbestos family, along with elemental constituents including O, Mg, Al, Si, while in sample four K was also present. Among these, Al and Si are of particular concern due to their potential contribution to toxic exposure pathways. SEM images provided valuable morphological insights, confirming the presence of chrysotile with its characteristic fibrillar structure, antigorite in a laminar form and lizardite in microplate aggregates. These observations are consistent with and reinforce the findings from XRD analysis.

Sample 4, obtained from sedimentary and metamorphic formations, exhibited a mineral assemblage dominated by silicate minerals—especially sheet silicates—that may influence the physicochemical behavior of the material. Furthermore, the mineralogical composition of sample 4 included foliated and crystalline phases such as muscovite (in sheet form), kaolinite (as a secondary alteration product) and quartz (with sharp-edged and broken grains). This mineral assemblage is indicative of a geologically altered material, most likely of sedimentary origin, which has undergone physical and chemical erosion processes.

Overall, the results highlight the environmental and health significance of asbestos-containing formations in the Bajgora region and underline the need for continuous monitoring, risk assessment and possible remediation strategies in the affected areas.

6. Recommendations

Based on the findings of this study and the confirmed presence of hazardous asbestos minerals in the Bajgora region, the following measures are recommended to protect public health and ensure environmental safety:

- Designate the area for Health Risk Monitoring, given the confirmed presence of fibrous minerals from the asbestos group, such as chrysotile, which is known as a mineral with carcinogenic potential, particularly affecting the lungs.
- Implement continuous air quality monitoring to detect airborne asbestos fibers, which pose an inhalation hazard to the local population and workers.

- Establish regulatory criteria in accordance with national and international standards for construction, demolition, and recreational use of the area to minimize asbestos exposure.
- Monitor high-risk activities such as road construction, rock excavation, and infrastructure development that may disturb asbestos-bearing formations and release fibers into the air.
- Inform and educate the local population about the health risks associated with asbestos exposure, with a focus on preventive behaviors and community awareness campaigns.
- Enforce strict use of personal protective equipment (PPE) and compliance with occupational health and safety guidelines for all individuals working in or around the affected area.
- Assess the risk of asbestos dispersion from natural processes, such as erosion, runoff, and groundwater movement, which may contribute to environmental contamination.
- Develop a comprehensive Risk Management and Protection Plan for the Bajgora region, including mitigation measures, monitoring protocols, and public health strategies to safeguard the population and the environment.
- Establish a national database of geological formations containing asbestos, where, within the framework of land-use planning, the risk assessment that will arise from this activity is carried out.
- Initiate preventive health screening programs, especially chest radiography and pulmonary function tests, for the populations in these villages.
- Establish warning signs for asbestos exposure and develop culturally appropriate community awareness campaigns about the risk in the Bajgora region.

Author Contributions: Bahri Sinani.: conceptualization of paper; sampling, investigation of existing data; writing—original draft. B.B.: methodology; analysis determination, review of paper. A.A.R.: sampling location, data curation; laboratory analysis, review of analysis. Berat Sinani: sampling, sample preparation; laboratory analysis and data interpretation, I.B.: conceptualization; supervision; validation; reviewing and editing of paper. All authors have read and agreed to the published version of the manuscript.

Funding: This research received no external funding.

Data Availability Statement: The obtained data can be made available on request of interested parties.

Conflicts of Interest: The authors declare no conflicts of interest.

References

1. Wilk, E.; Krówczyńska, M.; Zagajewski, B. Modelling the Spatial Distribution of Asbestos—Cement Products in Poland with the Use of the Random Forest Algorithm. *Sustainability* **2019**, *11*, 4355. https://doi.org/10.3390/su11164355.
2. Peña-Castro, M.; Montero-Acosta, M.; Saba, M. A critical review of asbestos concentrations in water and air, according to exposure sources. *Heliyon* **2023**, *9*, e15730. https://doi.org/10.1016/j.heliyon.2023.e15730.
3. Virta, R.L. *Asbestos: Geology, Mineralogy, Mining, and Uses*; 2002, (USGS), https://doi.org/10.3133/ofr02149.
4. Visonà, S.D.; Capella, S.; Bodini, S.; Borrelli, P.; Villani, S.; Crespi, E.; Frontini, A.; Colosio, C.; Belluso, E. Inorganic Fiber Lung Burden in Subjects with Occupational and/or Anthropogenic Environmental Asbestos Exposure in Broni (Pavia, Northern Italy): An SEM-EDS Study on Autoptic Samples. *Int. J. Environ. Res. Public Health* **2021**, *18*, 2053. https://doi.org/10.3390/ijerph18042053.

5. Punturo, R.; Ricchiuti, C.; Giorno, E.; Apollaro, C.; Miriello, D.; Visalli, R.; Bloise, A.; Rita, P.M.; Cantaro, C. Potentially toxic elements (PTES) in actinolite and serpentinite host rocks: A case study from the Basilicata Region (Italy). *Ofioliti* **2023**, *48*, 75–151.
6. Clin, B.; Gramond, C.; Delva, F.; Andujar, P.; Thaon, I.; Brochard, P.; Benoist, J.; Gislard, A.; Laurent, F.; Benlala, I.; et al. Asbestos exposure, pleural plaques and digestive cancers. *BMC Public Health* **2025**, *25*, 686. https://doi.org/10.1186/s12889-025-21969-0.
7. Bloise, A.; Kusiorowski, R.; Gualtieri, A.F. The Effect of Grinding on Tremolite Asbestos and Anthophyllite Asbestos. *Minerals* **2018**, *8*, 274. https://doi.org/10.3390/min8070274.
8. Lysaniuk, B.; Cely-García, M.F.; Giraldo, M.; Larrahondo, J.M.; Serrano-Calderón, L.M.; Guerrero-Bernal, J.C.; Briceno-Ayala, L.; Cruz Rodriguez, E.; Ramos-Bonilla, J.P. Using GIS to Estimate Population at Risk Because of Residence Proximity to Asbestos Processing Facilities in Colombia. *Int. J. Environ. Res. Public Health* **2021**, *18*, 13297. https://doi.org/10.3390/ijerph182413297.
9. Feder, I.S.; Tischoff, I.; Theile, A.; Schmitz, I.; Merget, R.; Tannapfel, A. The asbestos fibre burden in human lungs: New insights into the chrysotile debate. *Eur. Respir. J.* **2017**, *49*, 1602534. https://doi.org/10.1183/13993003.02534-2016.
10. Wilson, R.; McConnell, E.E.; Ross, M.; Axten, C.W.; Nolan, R.P. Risk assessment due to environmental exposures to fibrous particulates associated with taconite ore. *Regul. Toxicol. Pharmacol.* **2008**, *52*, S232–S245. https://doi.org/10.1016/j.yrtph.2007.11.005.
11. Bloise, A.; Ricchiuti, C.; Punturo, R.; Pereira, D. Potentially toxic elements (PTEs) associated with asbestos chrysotile, tremolite and actinolite in the Calabria region (Italy). *Chem. Geol.* **2020**, *558*, 119896.
12. Krówczyńska, M.; Wilk, E. Environmental and Occupational Exposure to Asbestos as a Result of Consumption and Use in Poland. *Int. J. Environ. Res. Public Health* **2019**, *16*, 2611. https://doi.org/10.3390/ijerph16142611.
13. Virta, R.L. Worldwide Asbestos Supply and Consumption Trends from 1900 Through (2003); USGS; https://doi.org/10.3133/cir1298.
14. Baumann, F.; Buck, B.J.; Metcalf, R.V.; McLaurin, B.T.; Merkler, D.J.; Carbone, M. The Presence of Asbestos in the Natural Environment is Likely Related to Mesothelioma in Young Individuals and Women from Southern Nevada. *J. Thorac. Oncol.* **2015**, *10*, 731–737. https://doi.org/10.1097/JTO.0000000000000506.
15. Zarezadeh, E.; Jonidi Jafari, A.; Gholami, M.; Farzadkia, M.; Ashouri, E.; Shahsavani, A.; Kermani, M.; Nakhjirgan, P. A comprehensive study on the spatial and temporal variation of BTEX and asbestos in the northwest of Iran: Human risk assessment. *Heliyon* **2024**, *10*, e31640. https://doi.org/10.1016/j.heliyon.2024.e31640.
16. Sinani, B.; Boev, B.; Reka, A.; Boev, I.; Sinani, B.; Lecaj, E. Statistical and chemical analysis of soil pollution from koshtova landfill Mitrovice—Kosovo. *Int. Multidiscip. Sci. GeoConference SGEM* 2024, *3*, 329–336. https://doi.org/10.5593/sgem2024/3.1/s13.40.
17. Curtis, W.N. Environmental asbestos exposure and risk of mesothelioma. *Ann. Transl. Med.* **2017**, *5*, 234. https://doi.org/10.21037/atm.2017.03.74.
18. Millette, J. Asbestos Analysis Methods. In *Asbestos*; CRC Press: Boca Raton, FL, USA, 2005; pp. 9–37. https://doi.org/10.1201/9781420038149.ch2.
19. Gogou, E.; Hatzoglou, C.; Siachpazidou, D.; Zarogiannis, S.G.; Gourgoulianis, K.I. Asbestos Ban Policies and Mesothelioma Mortality in Greece. *BMC Public Health* **2023**, *24*, 1177. https://doi.org/10.21203/rs.3.rs-3369279/v1.
20. Jana. D. Sample preparation techniques in petrographic examinations of construction materials: A state-of-the-art review. In Proceedings of the Twenty-Eighth Conference on Cement Microscopy, Denver, CO, USA, 30 April–4 May 2006.
21. Sinani, B.; Boev, B.; Reka, A.; Boev, I.; Pacarizi, M.; Qeriqi, E. Geo-statistical analysis of distribution of as, Fe, Mn, Cu, and Zn in Artana mine tailing from floating process. *Int. Multidiscip. Sci. GeoConference: SGEM* **2023**, *23*, 171–178. https://doi.org/10.5593/sgem2023/2.1/s08.22.
22. Ali, A.; Zhang, N.; Santos, R.M. Mineral Characterization Using Scanning Electron Microscopy (SEM): A Review of the Fundamentals, Advancements, and Research Directions. *Appl. Sci.* **2023**, *13*, 12600. https://doi.org/10.3390/app132312600.
23. Bukleski, M.; Dimitrovska-Lazova, S.; Aleksovska, S. Temperature dependent phase transitions and their relation to isosbestic point formation. Case study of C(NH2)3PbI3. *Spectrochim. Acta Part A Mol. Biomol. Spectrosc.* **2022**, *266*, 120462. https://doi.org/10.1016/j.saa.2021.120462.
24. United States Environmental Protection Agency; (1993); Method for the determination of asbestos in bulk building materials (EPA/600/R-93/116); Office of Research and Development, Washington, DC.
25. Gualtieri, F.A.; Gandolfi, B.N.; Passaglia, E.; Pollastri, S.; Mattioli, M.; Giordani, M.; Ottaviani, M.F.; Cangiotti, M.; Bloise, A.; Barca, D.; et al. Is fibrous ferrierite a potential health hazard? Characterization and comparison with fibrous erionite. *Am. Mineral.* **2018**, *103*, 1044–1055. https://doi.org/10.2138/am-2018-6508.

26. Gualtieri, F.A. Towards a quantitative model to predict the toxicity/pathogenicity potential of mineral fibers. *Toxicol. Appl. Pharmacol.* **2018**, *361*, 89–98. https://doi.org/10.1016/j.taap.2018.05.012.
27. Meholli, B.; Milushi, I.; Kodra, A. *Ophiolitic Magmatism and New Magmatism in the Bajgora Region, Mineral Resources Associated with Them*; 2014, Doctoral Thesis, Polytechnic University of Tirana, Tiranë, Albania
28. Boev, B.; Jovanovski, G.; Makreski, P. Minerals from Macedonia. XX. Geological Setting, Lithologies, and Identification of the Minerals from Rzanovo Fe-Ni Deposit. *Turk. J. Earth Sci.* **2009**, *18*, 631–652. https://doi.org/10.3906/yer-0710-1.
29. Zichella, L.; Baudana, F.; Zanetti, G.; Marini, P. Vinyl-Asbestos Floor Risk Exposure in Three Different Simulations. *Int. J. Environ. Res. Public Health* **2021**, *18*, 2073. https://doi.org/10.3390/ijerph18042073.
30. Beak Consultants GmbH. *Geological Map of Kosovo (Scale 1:200,000)*; Independent Commission for Mines and Minerals (ICMM): Pristina, Kosovo, 2006.
31. Nath, F.; Asish, S.; Sutradhar, S.; Li, Z.; Shahadat, N.; Debi, H.R.; Shamsul Hoque, S.M. Rock Thin-section Analysis and Mineral Detection Utilizing Deep Learning Approach. In Proceedings of the 11th Unconventional Resources Technology Conference, Denver, CO, USA, 13–15 June 2023. https://doi.org/10.15530/urtec-2023-3865660.
32. Heikal, M.T.S.; Surour, A.A.; Said, A.A. Chemical, thermal and infra-red characterization of chrysotile modes from the Wadi Daftah serpentinite (Semail ophiolite), United Arab Emirates. *Discov. Geosci.* **2024**, *2*, 87. https://doi.org/10.1007/s44288-024-00087-1.
33. Shaban, S.E.; Ibrahiem, N.M.; El-mongy, S.A.; Elshereafy, E.E. Validation of scanning electron microscope (SEM), energy dispersive X-ray (EDX) and gamma spectrometry to verify source nuclear material for safeguards purposes. *J. Radioanal. Nucl. Chem.* **2013**, *296*, 1219–1224.
34. Sinani, B.; Elezaj, Z.; Peci, N.; Sinani, B. Engineering geological studies on zhur dam. *Int. Multidiscip. Sci. GeoConference: SGEM* **2015**, *1*, 299–305.
35. Baumann, F.; Ambrosi, J.P.; Carbone, M. The presence of asbestos in the natural environment is still a public health hazard. *J. Toxicol. Environ. Health Part B* **2015**, *18*, 231–252.
36. Miller, A.; Wiens, M. Naturally Occurring Asbestos in an Outdoor Setting. National Collaborating Centre for Environmental Health. 2018. Available online: https://ncceh.ca/sites/default/files/Naturally_occurring_asbestos_outdoor_setting-Feb_2018.pdf (accessed on 23.03.25).
37. California Department of Toxic Substances Control. Guidance for School Sites with Naturally Occurring Asbestos. California Environmental Protection Agency, DTSC. 2018. Available online: https://dtsc.ca.gov/wp-content/uploads/sites/31/2018/09/SMBRP_POL_Guidance_Schools_NOA.pdf (accessed on 14.06.2025).
38. Pennsylvania Department of Health. Naturally Occurring Asbestos: Frequently Asked Questions. 2023. Available online: https://www.pa.gov/content/dam/copapwp-pagov/en/health/documents/topics/documents/environmental-health/NOA%20Frequently%20Asked%20Questions.pdf (accessed on 14.06.2025).
39. US Department of Agriculture, Forest Service. Naturally Occurring Asbestos on National Forest Lands. 2022. Available online: https://www.fs.usda.gov/r05/safety-ethics/naturally-occurring-asbestos (accessed on 10.03.2025).